Momentum distribution in nuclear matter and finite nuclei

H. Müther and G. Knehr

Institut für Theoretische Physik, Universität Tübingen, Auf der Morgenstelle 14, D-72076 Tübingen, Germany

A. Polls

Departament d'Estructura i Constituents de la Matèria, Universitat de Barcelona, Diagonal 647, E-08028 Barcelona, Spain

A simple method is presented to evaluate the effects of short-range correlations on the momentum distribution of nucleons in nuclear matter within the framework of the Green's function approach. The method provides a very efficient representation of the single-particle Green's function for a correlated system. The reliability of this method is established by comparing its results to those obtained in more elaborate calculations. The sensitivity of the momentum distribution on the nucleon-nucleon interaction and the nuclear density is studied. The momentum distributions of nucleons in finite nuclei are derived from those in nuclear matter using a local-density approximation. These results are compared to those obtained directly for light nuclei like ^{16}O.

I. INTRODUCTION

Realistic nucleon-nucleon (NN) interactions like the phenomenological Reid soft-core potential [1] or one-boson-exchange (OBE) potentials [2], which are adjusted to fit the NN scattering data, typically contain rather strong short-range components. These short-range parts as well as a non-negligible tensor component are responsible for the fact that simple mean-field or Hartree-Fock (HF) calculations of nuclear systems yield very unsatisfactory results. It turns out that HF calculations using such realistic NN forces may not even lead to bound nuclei [3]. Therefore, based on these theoretical considerations it seems obvious that nuclear wave functions must contain correlations, which are induced by these short-range and tensor components and cannot be accounted for in the mean-field or HF approximation to the solution of the many-body problem.

The question is whether there exist experimental observables which reflect these correlations in an unambiguous way. In particular it would be nice if one could explore these correlations in terms of single-nucleon observables since they are easier to measure as well as to calculate. This leads to the question of how correlations affect the single-particle density $\rho(r,r')$ in the nuclear many-body system. Rather than discussing this nonlocal representation of the density matrix, we may consider as well its Wigner transform [4] $f(R,k)$. Integrating this Wigner distribution over all momenta k yields the local density $\rho(r=r')$. This local-density distribution, or to be more precise the corresponding charge distribution, has been investigated with high precision in elastic electron scattering experiments [5]. Also the matter distribution can be analyzed in a rather model-independent way by means of elastic α scattering and other probes [6]. It seems, however, that these "experimental" charge and matter distributions can very well be reproduced within a mean-field approximation for the nuclear wave function.

Integrating the Wigner transform of the one-nucleon density matrix over all spatial coordinates one obtains the momentum distribution $n(k)$. For an infinite system, invariant under local transformations, the mean-field or Hartree-Fock prediction for this momentum distribution is identical to the momentum distribution of a free Fermi gas. This means that all states with momenta less than the Fermi momentum k_F are occupied with a probability $n=1$, while all states with momenta k above k_F are completely unoccupied ($n=0$). Correlations beyond the HF approach modify this momentum distribution in the sense that states with momenta below k_F are partly depleted, whereas states with high momenta are partly occupied.

From these considerations for the infinite system of nuclear matter one may expect that correlations beyond HF will enhance the momentum distribution at high momenta k also for finite nuclei. This is one reason why modern electron accelerators have been used to explore the momentum distribution of nucleons in nuclei by means of nucleon knockout, $(e,e')p$, experiments [7–9].

Microscopic nuclear structure calculations which account for the effects of short-range and tensor correlations of realistic NN interactions are mainly performed for very light nuclei [10–13] or infinite nuclear matter [14–21]. From these results for nuclear matter one then tries to extract the effects of NN correlations in order to estimate their influence on the momentum distribution of real nuclei using a local-density approximation (LDA) [22–24].

Recently, there have also been attempts to determine the momentum distribution in a microscopic calculation considering directly finite nuclei such as ^{16}O [25–27]. It turns out that the Green's function approach is particularly useful for these investigations. This method not only provides the total momentum distribution but also yields detailed information on the spectral function. This spectral function contains the information at which excitation of the residual nucleus or, using the nomenclature of the knockout experiment, at which missing energy the various components of the momentum distribution should be observed. These studies predict that high-momentum components in the momentum distribution due to short-range correlations should show up preferentially at large missing energies.

The comparison of the momentum distributions obtained within the Green's function approach for ^{16}O with corresponding ones for nuclear matter exhibited remarkable discrepancies [27]. Therefore the question arises if these discrepancies demonstrate the limitation of the LDA in predicting the momentum distribution. As has been argued already in [27], such a conclusion would be premature since that comparison was plagued with various inconsistencies like, e.g., the following.

(i) The momentum distribution calculated for nuclear matter using the Green's function approach has been available only for one specific density, the saturation density of nuclear matter. This density may be too large to be typical for the situation of nuclei as small as ^{16}O.

(ii) The result for nuclear matter has been derived from a self-consistent calculation of the single-particle Green's function [18] whereas the calculation for the finite system has been performed considering contributions to the self-energy of the nucleons up to second order in a nuclear matter G matrix [27].

(iii) The calculation of the self-energy for the nucleons in the finite system has been made employing a single-particle spectrum with a substantial gap at the Fermi surface, whereas a continuous prescription has been used for nuclear matter.

(iv) The calculation for the finite system was limited to partial waves with angular momenta $l \leq 3$. This limitation may be too severe for the momentum distribution at high momenta.

(v) While the Reid soft-core potential [1] has been used for the study of nuclear matter in [18] the OBE potential B of [2] has been employed for the calculation of ^{16}O.

It is one aim of the present investigation to remove some of the differences between these calculations of finite nuclei and infinite nuclear matter. Furthermore, we want to study the sensitivity of the calculated momentum distributions in the nuclear systems on the nuclear density, the NN interaction considered, and various other ingredients of the many-body calculation. For that purpose we have developed a new very efficient method to calculate the momentum distribution in nuclear matter using an approximation to the Green's function method very similar to the one presented in [27] for finite nuclei. The comparison of results obtained with this approximation scheme with those resulting from the much more sophisticated scheme of [18] demonstrates the reliability of the method developed here. The efficiency of the new
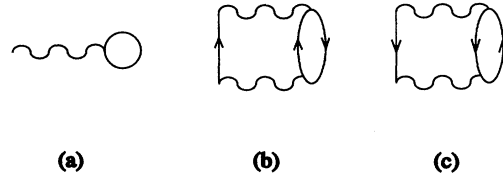

(a)   **(b)**   **(c)**

FIG. 1. Graphical representation of the Hartree-Fock (a), the two-particle–one-hole (2p1h) (b), and the two-hole–one-particle contribution (2h1p) (c) to the self-energy of the nucleon.

scheme allows the detailed studies mentioned above.

After this Introduction, Sec. II of this paper describes the technique to be used for studies of nuclear matter. In particular we will also present an efficient representation of the single-particle Green's function, which allows a self-consistent treatment. In Sec. III we briefly review the basic approximations used in the calculation of the momentum distribution for finite nuclei of [27] and we outline a method to determine this momentum distribution, in which the mean-field part is calculated for the finite system but the effects of correlations are taken from nuclear matter at various densities, using a LDA. The results of the numerical calculations are presented in Sec. IV. In this section we discuss the sensitivity of the results in nuclear matter on the various ingredients. Also we compare the predictions of the LDA with results obtained by the method of [27]. For that purpose we extended the studies of [27] by considering different interactions and allowing for higher partial waves. The main conclusions are summarized in Sec. V.

II. MOMENTUM DISTRIBUTION IN NUCLEAR MATTER

A. Self-energy and Dyson equation

Our calculation of the single-particle Green's function for nucleons in nuclear matter is based on the definition of the self-energy of the nucleon, which includes the terms of first and second order in an effective interaction $\mathscr{V}$, which we will define below. The expression for the term of first order, displayed in Fig. 1(a), corresponds to the Hartree-Fock expression for the single-particle energy of a nucleon with momentum k in a system of nuclear matter with a Fermi momentum k_F:

$$\Sigma^{(\mathrm{HF})}(k) = \sum_{h < F} \langle kh \mid \mathscr{V} \mid kh \rangle$$

$$= \sum_{LSJT} (2J+1)(2T+1) \left\{ \Theta(k_F-k) \int_0^{1/2\,|k-k_F|} dq\, 8q^2 + \frac{1}{k} \int_{1/2\,|k-k_F|}^{1/2\,(k+k_F)} dq\, q[(k_F^2-q^2)-4q(q-k_F)] \right\}$$

$$\times \mathscr{V}_{LL}^{JST}(K_{\mathrm{av}};q,q). \tag{1}$$

In the second part of this equation the matrix elements of $\mathscr{V}$ are given using the conventional partial wave representation with L, S, J, and T denoting the orbital angular momentum for the relative motion, the spin, the total angular momentum and the isospin of the two interacting nucleons, respectively. The relative momentum q is diagonal and an average value K_{av} has been used for the c.m. momentum, which is given by [28]

$$K_{av}^2 = \begin{cases} k^2 + q^2 & \text{if} \quad 0 \le q \le \frac{1}{2}|k - k_F|, \\ \frac{3}{4}k^2 - qk + \frac{1}{4}k_F^2 & \text{if} \quad \frac{1}{2}|k - k_F| \le q \le \frac{1}{2}(k + k_F). \end{cases} \tag{2}$$

The term of second order in the effective interaction with intermediate two-particle–1-hole (2p1h) states, displayed in Fig. 1(b), also depends on the energy ω of the nucleon under consideration and can be calculated according to

$$\Sigma^{(2p1h)}(k, \omega) = \sum_{h < F} \sum_{p_1, p_2 > F} \frac{\langle kh | \mathscr{V} | p_1, p_2 \rangle^2}{\omega - (\epsilon_{p1} + \epsilon_{p2} - \epsilon_h) + i\eta}$$

$$= \sum_{LSJT} (2J+1)(2T+1) \left\{ \Theta(k_F - k) \int_0^{1/2|k-k_F|} dq\, 8q^2 + \frac{1}{k} \int_{1/2|k-k_F|}^{1/2(k+k_F)} dq\, q[(k_F^2 - q^2) - 4q(q - k_F)] \right\}$$

$$\times \left[\sum_{L'} \int_0^\infty dq'\, q'^2 \frac{Q(K_{av}, q')\mathscr{V}_{LL'}^{JST}(K_{av}; q, q')^2}{\omega - E_{2p1h}(K_{av}, q, q') + i\eta} \right]. \tag{3}$$

The single-particle energies ϵ_q correspond to the Hartree-Fock approximation for the single-particle energy,

$$\epsilon_q = \frac{q^2}{2m} + \Sigma^{(HF)}(q), \tag{4}$$

with m for the mass of the nucleon. In the second part of Eq. (3) we have used the so-called angle-averaged approximation for the Pauli operator, which is defined by [28]

$$Q(K, q) = \begin{cases} 0 & \text{if} \quad q \le \sqrt{k_F^2 - K^2}, \\ \dfrac{K^2 + q^2 - k_F^2}{2Kq} & \text{if} \quad \sqrt{k_F^2 - K^2} \le q \le k_F + K, \\ 1 & \text{if} \quad q \ge k_F + K. \end{cases} \tag{5}$$

The other contribution to the second order self-energy with intermediate two-hole–one-particle states (2h1p), displayed in Fig. 1(c), can be calculated in a way very similar to Eq. (3)

$$\Sigma^{(2h1p)}k, \omega = \sum_{p > F} \sum_{h_1, h_2 < F} \frac{\langle kp | \mathscr{V} | h_1, h_2 \rangle 2}{\omega - (\epsilon_{h1} + \epsilon_{h2} - \epsilon_p) - i\eta}$$

$$= \sum_{LL'SJT} \int_0^\infty dq\, W(q) \int_0^\infty dq'\, q'^2 \frac{P(\tilde{K}_{av}, q')\mathscr{V}_{LL'}^{JST}(\tilde{K}_{av}; q, q')^2}{\omega - E_{2h1p}(\tilde{K}_{av}, q, q') - i\eta}. \tag{6}$$

The Pauli operator Q, which ensured in Eq. (3) that the sum over intermediate two-particle states is restricted to states above the Fermi surface, is replaced by a corresponding operator P to ensure that the intermediate two-hole states are below the Fermi level:

$$P(K, q) = \begin{cases} 0 & \text{if} \quad q \ge \sqrt{k_F^2 - K^2}, \\ \dfrac{k_F^2 - K^2 - q^2}{2Kq} & \text{if} \quad \sqrt{k_F^2 - K^2} \ge q \ge k_F - K, \\ 1 & \text{if} \quad q \le k_F - K. \end{cases} \tag{7}$$

The definitions of the mean value for the center of mass momentum, $\tilde{K}_{av}$, and the weight function $W(q)$ in the integral of Eq. (6) are a bit more involved than in the case of the 2p1h term and are given in the Appendix [29].

After the definition of the self-energy we could now proceed and calculate the corresponding single-particle Green's function by solving a Dyson equation of the form [30]

$$g(k, \omega) = g^{(HF)}(k, \omega) + g^{(HF)}(k, \omega)[\Sigma^{(2p1h)}(k, \omega)$$

$$+ \Sigma^{(2h1p)}(k, \omega)]g(k, \omega), \tag{8}$$

with the single-particle Green's function in the Hartree-Fock approximation:

$$g^{(\mathrm{HF})}(k,\omega)=\frac{\Theta\ (k_F-k)}{\omega-\epsilon_k-i\,\eta}+\frac{\Theta\ (k-k_F)}{\omega-\epsilon_k+i\,\eta}\ . \qquad (9)$$

The momentum distribution $n(\mathrm{k})$ can then be calculated from the imaginary part of the single-particle Green's function by

$$n(\mathrm{k})=\frac{1}{\pi}\int_{-\infty}^{\epsilon_F}d\omega\,\mathrm{Im}g(k,\omega). \qquad (10)$$

B. Numerical approach

Instead of proceeding along the lines indicated in Eqs. (8)–(10), we use the fact that in all numerical calculations the integrals of Eqs. (3) and (6) will be discretized. This means that Eq. (3) takes the form

$$\Sigma^{(2\mathrm{p}1\mathrm{h})}(k,\omega)=\sum_{i=1}^{N}\frac{F_i^2(k)}{\omega-E_i^{(2\mathrm{p}1\mathrm{h})}+i\,\eta}, \qquad (11)$$

while Eq. (6) can be rewritten as

$$\Sigma^{(2\mathrm{h}1\mathrm{p})}(k,\omega)=\sum_{j=1}^{M}\frac{G_j^2(k)}{\omega-E_j^{(2\mathrm{h}1\mathrm{p})}-i\,\eta}. \qquad (12)$$

This discretization implies in particular that we represent the singularities of the self-energy in terms of discrete poles slightly above (2h1p) and below (2p1h) the real axes. This analytic structure of the self-energy is identical to the one obtained for a finite system within a model space defined in terms of discrete single-particle states. This means that we may use the same techniques to determine the features of the single-particle Green's function as employed, e.g., in [31,32]. Translating this technique into the present example, this means that the single-particle Green's function will be defined in the Lehmann representation by

$$g(k,\omega)=\sum_{\alpha=1}^{N+M+1}\frac{X_\alpha^2}{\omega-\omega_\alpha\pm i\,\eta}, \qquad (13)$$

with the sign in front of the infinitesimal imaginary part η being positive for poles ω_α above the Fermi energy E_F and negative else. For each k the positions of these poles, ω_α, and the residua, X_α^2, can be determined from the solution of the following eigenvalue problem:

$$\begin{pmatrix} \epsilon_k & F_1 & \ldots & F_N & G_1 & \ldots & G_M \\ F_1 & E_1^{(2\mathrm{p}1\mathrm{h})} & & 0 & & & \\ \vdots & & \ddots & & & & \\ F_N & 0 & & E_N^{(2\mathrm{p}1\mathrm{h})} & & & \\ G_1 & & & & E_1^{(2\mathrm{h}1\mathrm{p})} & & \\ \vdots & & & & & \ddots & \\ G_M & 0 & \ldots & 0 & & & E_M^{(2\mathrm{h}1\mathrm{p})} \end{pmatrix} \begin{pmatrix} X_\alpha \\ Y_{\alpha,1} \\ \vdots \\ Y_{\alpha,N} \\ Z_{\alpha,1} \\ \vdots \\ Z_{\alpha,M} \end{pmatrix} = \omega_\alpha \begin{pmatrix} X_\alpha \\ Y_{\alpha,1} \\ \vdots \\ Y_{\alpha,N} \\ Z_{\alpha,1} \\ \vdots \\ Z_{\alpha,M} \end{pmatrix}. \qquad (14)$$

Note that the dimension of this matrix $(N+M+1)$ as well as the matrix elements F_i, $E_i^{(2\mathrm{p}1\mathrm{h})}$ and G_j, $E_j^{(2\mathrm{h}1\mathrm{p})}$ refer to the nomenclature employed in Eqs. (11) and (12), respectively. Using the representation of the Green's function in Eq. (13) the occupation probabilities are calculated easily as

$$\tilde{n}(k)=\sum_\alpha\Theta(E_F-\omega_\alpha)X_\alpha^2, \qquad (15)$$

which leads to the momentum distribution if we divide by the single-particle density,

$$n(k)=\frac{\tilde{n}(k)}{\rho}=\frac{3\tilde{n}(k)}{4\pi k_F^3}, \qquad (16)$$

with k_F the Fermi momentum of the nuclear matter system.

C. BAGEL approximation

Using the Lehmann representation of the single-particle Green's function of Eq. (13) the continua of states of nuclear matter with one additional nucleon and one hole are represented in terms of some discrete energies ω_α. Depending on the accuracy of the discretization on Eqs. (11) and (12) the number of eigenvalues typically considered in numerical calculations ranges from a few hundred up to a few thousand. This may be compared to the Hartree-Fock approximation of Eq. (9), in which the Green's function for a nucleon with momentum k is represented by just one pole. This number of pole terms is not a problem as long as one is just interested in the evaluation of the Green's function or simple observables as the momentum distribution. The structure of the Green's function in Eq. (13), however, may be too complicated to be used in the evaluation of quantities which are defined in terms of products of these Green's functions. Examples for such quantities are, e.g., the various response functions of nuclear matter or a self-consistent evaluation of the self-energy, which implies that the self-energies to be used in the

Dyson equation (8) are calculated in terms of the resulting Green's functions. For such calculations it may be preferable to "optimize" the number of pole terms in Eq. (13), which means trying to find a minimum number of poles, which yields the same observables than the complete Green's function.

In order to develop such an efficient representation of the Green's function we try to apply the so-called "basis generated by Lanczos" (BAGEL) scheme, which has successfully been used for the description of finite nuclei in finite model spaces [31–33]. For that purpose we consider the operator $\hat{a}$ which corresponds to a part of the matrix in Eq. (14),

$$
\hat{a} = \begin{pmatrix} \epsilon_k & F_1 & \dots & F_N \\ F_1 & E_1^{(2p1h)} & & \\ \vdots & & \ddots & \\ F_N & & & E_N^{(2p1h)} \end{pmatrix}, \tag{17}
$$

and apply this operator on the single-particle state $|\alpha\rangle$ which in terms of the matrix representation of Eq. (17) is described by the column vector $(1,0,\dots,0)^T$,

$$
\hat{a}|\alpha\rangle = \epsilon_k|\alpha\rangle + \tilde{a}_1|\alpha_1\rangle, \tag{18}
$$

where $|\alpha_1\rangle$ is orthogonal to $|\alpha\rangle$ and the coefficient $\tilde{a}_1$ is chosen so that $|\alpha_1\rangle$ is normalized. Following the Lanczos algorithm [34], one can subsequently construct additional states $|\alpha_i\rangle$, which are all orthogonal to each other. Applying the Lanczos procedure n times one obtains n basis states of the 2p1h configuration space.

In a similar way we can furthermore construct m basis states of the 2h1p configuration space by considering the corresponding submatrix of Eq. (14)

$$
\hat{A} = \begin{pmatrix} \epsilon_k & G_1 & \dots & G_N \\ G_1 & E_1^{(2h1p)} & & \\ \vdots & & \ddots & \\ G_M & & & E_M^{(2h1p)} \end{pmatrix}, \tag{19}
$$

and reduce the eigenvalue problem of Eq. (14) to the corresponding one in the subspace defined by the basis of the single-particle state plus the $(n+m)$ basis states generated by the Lanczos scheme just outlined. The Green's function of this BAGEL(n,m) approximation is then defined according to Eq. (13) using the $(n+m+1)$ eigenvalues and vectors obtained from the diagonalization of the matrix truncated to the subspace. It is obvious that the BAGEL(0,0) corresponds to the HF approximation, while for n approaching N and m close to M the BAGEL(n,m) approximation for the Green's function becomes identical to the exact solution of Eqs. (14) and (13).

D. Effective interaction

At the end of this section we want to define the effective NN interaction $\mathscr{V}$, used in the definition of the self-energy above. One possible choice would be of course to replace $\mathscr{V}$ by the bare NN interaction. As has been discussed already in the Introduction, the HF approximation in terms of a re-alistic NN interaction is not a very useful approach and it is not clear whether a perturbation expansion in terms of the bare NN interaction up to second order, as just outlined, will be sufficient. Therefore we employ the G matrix, an appropriate solution of the Bethe-Goldstone equation for $\mathscr{V}$. The starting energy Z in the Bethe-Goldstone equation is chosen according to the Brueckner-Hartree-Fock (BHF) choice for the self-energy of a nucleon with momentum k below the Fermi momentum and put to be the average of two single-particle states below the Fermi energy if k is above the Fermi momentum. This ensures that G remains real. With this choice we employ an approach which is very similar to the one used for finite nuclei in [27], where the self-energy is also calculated including terms up to second order in a nuclear matter G matrix.

Using the G matrix for the effective interaction also implies, however, that we have to face a double-counting problem. The diagram of second order, displayed in Fig. 1(b) is to some extent already taken into account in the Brueckner-Hartree-Fock approach for the self-energy displayed in Fig. 1(a). This double counting does not directly effect the calculation of the momentum distribution. The choice for the starting energy just presented leads to a real self-energy contribution of Eq. (1) without any poles and therefore the momentum distribution calculated for a self-energy, which only accounts for this term, remains identical to the HF one. There is a self-consistency problem, however, with respect to the energy spectrum reflected in the poles of the Green's function [see Eq. (13)]. If for the moment we ignore the 2h1p contribution to the self-energy and evaluate the Green's function according to scheme outlined in Eqs. (13) and (14) for a nucleon with momentum below k_F, we will find one eigenstate of Eq. (14) with negative energy and a large coefficient X_α, the quasihole state, and N eigenvalues at positive energies. Because of the diagonalization, however, the energy of the quasihole state, $\epsilon_k^{(qh,2p1h)}$, will be substantially below the corresponding HF energy ϵ_k. Therefore we replace the first element of the matrix in Eq. (14) by

$$
\epsilon_k \Rightarrow \tilde{\epsilon}_k = \epsilon_k - (\epsilon_k^{(qh,2p1h)} - \epsilon_k). \tag{20}
$$

This shift in energy ensures that the quasihole state for a self-energy with inclusion of only the 2p1h term will essentially be identical to the BHF energy. Therefore the double counting is removed. Note again that this double-counting problem does not affect the calculation of the momentum distribution. The energy shift is useful, however, to obtain a realistic energy spectrum for the poles of the Green's functions.

III. MOMENTUM DISTRIBUTION IN FINITE NUCLEI

A. Direct approach

Also the calculation of the momentum distribution presented in [26,27] directly for the nucleus ^{16}O is based on a self-energy of the nucleon calculated up to second order in a nuclear matter G matrix as described by the diagrams of Fig. 1. As a first step one considers the HF contribution to the self-energy:

$$\Sigma^{HF}_{l_1 j_1}(k_1, k'_1) = \frac{1}{2(2j_1+1)} \sum_{n_2 l_2 j_2 JT} (2J+1)(2T+1)\langle k_1 l_1 j_1 n_2 l_2 j_2 JT | G | k'_1 l_1 j_1 n_2 l_2 j_2 JT \rangle. \tag{21}$$

The matrix elements of G used in this expression are antisymmetrized NN matrix elements calculated in the laboratory system. The quantum numbers l_i and j_i refer to the orbital and total angular momentum of the single nucleons in this frame and J and T denote the angular momentum and isospin of the two-particle states. The matrix elements are calculated in a mixed representation with n_i referring to the radial quantum numbers of oscillator bound (hole) states, whereas the k_i denote the absolute value of the momentum for a free particle state. The summation over the oscillator quantum numbers is restricted to the states occupied in the independent particle model of ^{16}O. This Hartree-Fock part of the self-energy is real and does not depend on the energy. The HF single-particle wave functions can be obtained by expanding them,

$$|\alpha^{HF} l j m\rangle = \sum_i |K_i l j m\rangle \langle K_i | \alpha^{HF}\rangle_{lj}, \tag{22}$$

in a complete and orthonormal set of regular basis functions within a spherical box of radius R_{box} which is large as compared to the radius of the nucleus:

$$\Phi_{iljm}(\mathbf{r}) = \langle \mathbf{r} | K_i l j m\rangle = N_{il} j_l(K_i r) \mathscr{Y}_{ljm}(\vartheta \varphi). \tag{23}$$

In this equation $\mathscr{Y}_{ljm}$ represent the spherical harmonics including the spin degrees of freedom and j_l denote the spherical Bessel functions for the discrete momenta K_i which fulfill

$$j_l(K_i R_{box}) = 0. \tag{24}$$

Using the normalization constants

$$N_{il} = \begin{cases} \dfrac{\sqrt{2}}{\sqrt{R^3_{box}} j_{l-1}(K_i R_{box})} & \text{for } l>0, \\[2mm] \dfrac{i\pi\sqrt{2}}{\sqrt{R^3_{box}}} & \text{for } l=0, \end{cases} \tag{25}$$

the basis functions defined in Eq. (23) are orthogonal and normalized within the box. The expansion coefficients of Eq. (22) are obtained by diagonalizing the HF Hamiltonian:

$$\sum_{n=1}^{N_{max}} \langle K_i | \frac{K_i^2}{2m} \delta_{in} + \Sigma^{HF}_{lj} | K\rangle_n \langle K_n | \alpha^{HF}\rangle_{lj} = \epsilon^{HF}_{\alpha l j} \langle K_i | \alpha^{HF}\rangle_{lj}. \tag{26}$$

Here and in the following the set of basis states in the box has been truncated by assuming an appropriate N_{max}. From the HF wave functions and energies one can construct the HF approximation to the single-particle Green's function in the box [compare Eq. (9)], which for the finite nucleus has the form

$$g^{(HF)}_{\alpha l j}(k_i, k_j; \omega) = \frac{\langle k_i | \alpha^{HF}\rangle_{lj} \langle \alpha^{HF} | k_j\rangle_{lj}}{\omega - \epsilon^{HF}_{\alpha l j} \pm i\eta}. \tag{27}$$

As an example for the contributions to the self-energy of second order in G we recall the calculation of the 2p1h term. In the approach of [27] one first calculates the imaginary part of this self-energy contribution, depending on the energy ω,

$$W^{2p1h}_{l_1 j_1}(k_1, k'_1; \omega) = \frac{-1}{2(2j_1+1)} \sum_{n_2 l_2 j_2} \sum_{l_3 l_4 j_3 j_4} \sum_{JT} \int k_3^2 dk_3 \int k_4^2 dk_4 (2J+1)(2T+1)\langle k_1 l_1 j_1 n_2 l_2 j_2 JT | G | k_3 l_3 j_3 k_4 l_4 j_4 JT\rangle$$

$$\times \langle k_3 l_3 j_3 k_4 l_4 j_4 JT | G | k'_1 l_1 j_1 n_2 l_2 j_2 JT\rangle \pi\delta\left(\omega + \epsilon_{n_2 l_2 j_2} - \frac{k_3^2}{2m} - \frac{k_4^2}{2m}\right), \tag{28}$$

where the "experimental" single-particle energies $\epsilon_{n_2 l_2 j_2}$ are used for the hole states (-47 MeV, -21.8 MeV, -15.7 MeV for $s_{1/2}$, $p_{3/2}$, and $p_{1/2}$ states, respectively), while the energies of the particle states are given in terms of the kinetic energy only. The expression in Eq. (28) still ignores the requirement that the intermediate particle states must be orthogonal to the hole states, which are occupied for the nucleus under consideration. The techniques to incorporate the orthogonalization of the intermediate plane wave states to the occupied hole states as discussed in detail by Borromeo et al. [35] have also been used here. The 2h1p contribution to the imaginary part, $W^{2h1p}_{l_1 j_1}(k_1, k'_1; \omega)$, can be calculated in a similar way (see also [35]).

The choice to assume pure kinetic energies for the particle states in calculating the imaginary parts of W^{2p1h}[Eq. (28)] and W^{2h1p} may not be very realistic for the excitation modes at low energy. Indeed a sizable imaginary part in W^{2h1p} is obtained only for energies ω below -40 MeV. As we are mainly interested, however, in the effects of short-range correlations, which lead to excitations of particle states with high momentum, the choice seems to be appropriate. A different approach would be required to treat the coupling to the very low-lying two-particle–one-hole and two-hole–one-particle states in an adequate way. Attempts at such a treatment can be found in Refs. [36–38].

The real parts of the 2p1h and 2h1p terms in the self-energy can be calculated from the corresponding imaginary

parts by using dispersion relations [14]. As an example we present the dispersion relation for the 2p1h part, which is given by

$$V^{2p1h}_{l_1j_1}(k_1,k_1';\omega) = \frac{P}{\pi} \int_{-\infty}^{\infty} \frac{W^{2p1h}_{l_1j_1}(k_1,k_1';\omega')}{\omega'-\omega} d\omega', \quad (29)$$

where P means a principal value integral. Putting the various contributions together the correction to the HF self-energy due to the second order terms can be written

$$\Delta\Sigma_{lj}(k_1,k_2;\omega) = (V^{2p1h}-V_c+V^{2h1p})+i(W^{2p1h}+W^{2h1p}), \quad (30)$$

where V_c denotes a correction term to account for double counting between the V^{2p1h} and ladder contributions already contained in the HF part of the self-energy [27] (see also discussion at the end of Sec. II). With this correction to the self-energy one can solve a Dyson equation for the complete Green's function [see also Eq. (8)], which corresponds to an integral equation for finite systems:

$$g_{lj}(k_1,k_2;\omega) = g^{(HF)}_{lj}(k_1,k_2;\omega) + \int dk_3 \int dk_4 \, g^{(HF)}_{lj}(k_1,k_3;\omega)\Delta\Sigma_{lj}(k_3,k_4;\omega) \, g_{lj}(k_4,k_2;\omega). \quad (31)$$

From the imaginary part of this Green's function one can finally evaluate the momentum distribution according to

$$n(k) = \sum_{lj} 2(2j+1) \int_{-\infty}^{\epsilon_F} d\omega \, \frac{1}{\pi} \text{Im}[g_{lj}(k,k;\omega)]. \quad (32)$$

B. Local density approximation

Instead of evaluating the momentum distribution directly for the finite nucleus one can try to deduce the effects of correlations on the momentum distribution from the investigation of nuclear matter. As a first step towards such an approach we consider the local density $\rho^{HF}(r)$ and the momentum distribution $n^{HF}(k)$ derived from the solution of the Hartree-Fock equation (26). Using this density distribution we can define a local Fermi momentum

$$k^{local}_F(r) = \left[\frac{3\pi^2\rho^{HF}(r)}{2}\right]^{1/3} \quad (33)$$

and evaluate an average occupation number for the states occupied in the mean-field approach by

$$N_{aver} = \frac{4\pi}{A} \int r^2 dr \rho^{HF}(r)\bar{n}(k^{local}_F(r)), \quad (34)$$

with A the number of nucleons ($A=16$ in our example of ^{16}O) and $\bar{n}$ the occupation number [see Eq. (15)] calculated for nuclear matter with the local Fermi momentum and averaged over all momenta below this Fermi momentum. With this average occupation number one can account for the depletion of the occupation of states occupied in HF approximation. The high-momentum components originating from the partial occupation of states above the Fermi momentum are then evaluated as

$$\Delta n(k) = 4\pi k^2 \int 4\pi r^2 dr \Theta(k-k^{local}_F(r))n(k;k^{local}_F(r)), \quad (35)$$

where $n(k;k_F)$ is the momentum distribution of nuclear matter according to Eq. (16) calculated for the local Fermi momentum. The total momentum distribution is then given as

$$n^{LDA}(k) = N_{aver}n^{HF}(k) + \Delta n(k). \quad (36)$$

Within this local-density approximation we also would like to estimate the spectral strength which is missing in the calculation according to Eq. (32) due to a restriction in the sum of that equation to partial waves with orbital angular momentum up to $l=L_{max}$. For our LDA approximation that restriction would mean to consider contributions to $\Delta n(k)$ in Eq. (35) with

$$|\vec{l}| = rk \, \sin\varphi \leq \hbar \sqrt{L_{max}(L_{max}+1)}, \quad (37)$$

φ denoting the angle between r and the momentum k. This means that the integrand in Eq. (35) should be reduced by a factor

$$\frac{2}{\pi} \arcsin \frac{\hbar \sqrt{L_{max}(L_{max}+1)}}{rk}. \quad (38)$$

IV. RESULTS AND DISCUSSION

A. Nuclear matter

In order to evaluate the momentum distribution for nuclear matter at a given density ρ, which may as well be characterized by the corresponding Fermi momentum k_F, using the method outlined in the previous section, we have to determine as a first step the spectrum of HF single-particle energies ϵ_k. In our approach, defining the HF contribution to the self-energy [see Fig. 1(b)] in terms of the nuclear matter G matrix, these single-particle energies correspond to the single-particle energies obtained in the BHF approximation. For the OBE potential B of [2] the BHF single-particle energies have been parametrized [39] in terms of an effective mass m^* and a constant shift C by

$$\epsilon_k = \sqrt{k^2+m^{*2}} - m^* + m + C. \quad (39)$$

The parameters m^* and C as a function of the Fermi momentum k_F are listed in Table II of [39]. It should be men-
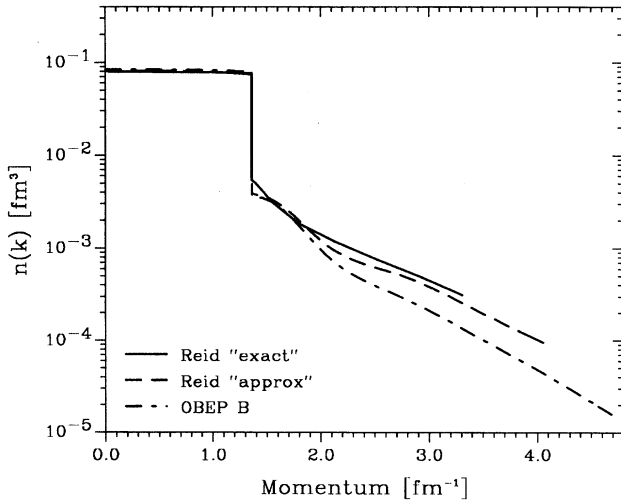
FIG. 2. Momentum distribution in nuclear matter at the empirical saturation density, k_F =1.36 fm^{-1}. Results obtained with the approximations discussed in Sec. II for the OBE potential B (dash-dotted line) and the Reid soft-core (dashed line) potentials are compared to the results using the Reid potential (solid line "exact") as derived from the more sophisticated calculations of Ref. [18].

tioned that in our study we have used the so-called nonrelativistic parametrization since in our present study we ignore all effects of the Dirac BHF approach due to a change of the Dirac spinors of the nucleons in the nuclear medium. With this definition of the single-particle spectrum one can evaluate the matrix in Eq. (14) with the renormalization of Eq. (20), solve the eigenvalue problem of Eq. (14), and determine the momentum distribution with Eq. (15).

Results for this momentum distribution in nuclear matter at the empirical saturation density (k_F=1.36 fm^{-1}) are dis-
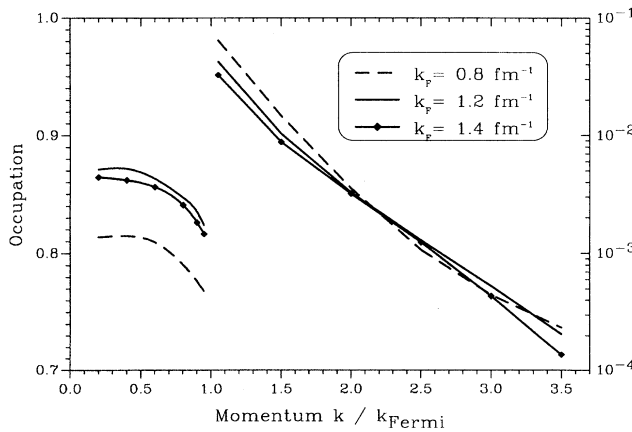

FIG. 3. Occupation probabilities in nuclear matter as a function of the momentum in units of the Fermi momentum k_F. Results obtained for the OBE potential B are shown for various densities (see description in the figure). The occupation probabilities for momenta below k_F are displayed with reference to the axis on the left side of the figure, while those for k larger k_F refer to the logarithmic scale on the axis at the right side.
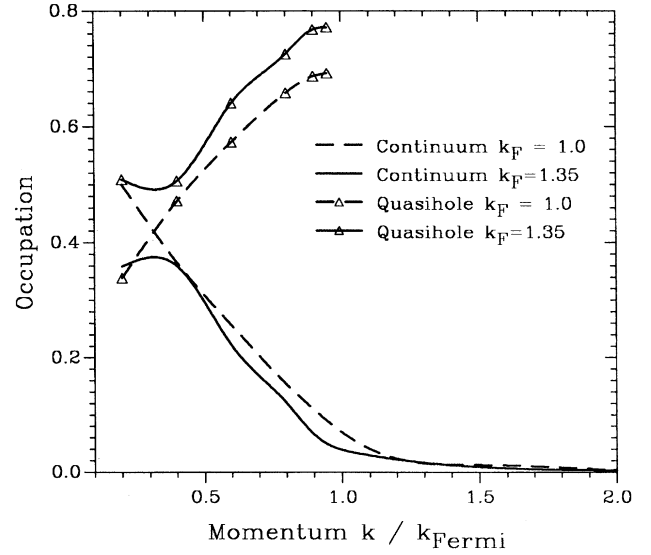

FIG. 4. The contribution of the quasihole state to the occupation probability [curves labeled with triangle; see Eq. (40)] and the continuum contribution as a function of the momentum k/k_f calculated for the OBE potential B. The dashed lines refer to a Fermi momentum of nuclear matter of 1.0 fm^{-1}, whereas the solid lines are obtained for k_F = 1.35 fm^{-1}.

played in Fig. 2. The momentum distribution derived from the OBE potential (dash-dotted line) is compared to the one obtained using the Reid soft-core potential employing the same technique (dashed line). The Reid soft-core potential predicts stronger effects of correlations in this momentum distribution. This is characterized by a stronger depletion of the states with momenta k below the Fermi momentum (the Reid soft core yields an average occupation of these states of 0.83 while the OBE potential predicts 0.86) as well as larger
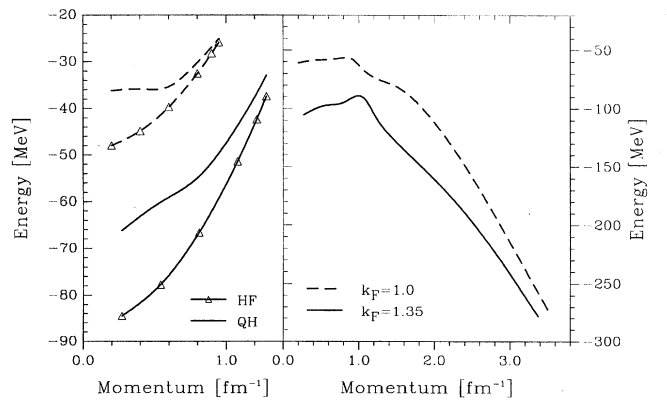

FIG. 5. Energy spectra for nuclear matter with Fermi momentum k_F = 1 fm^{-1} (dashed curves) and k_F = 1.35 fm^{-1} (solid lines) as a function of momentum. The left part of the figure exhibits the HF single-particle energies (curves labeled with triangles) and E_{qh} the energies of the quasihole states. In the right part the mean values $\bar{\omega}$ of the continuum part of the momentum distribution [see Eq. (42)] are displayed.

probability at higher momenta (for $k \approx 4$ fm^{-1} the density which is obtained for the Reid potential is by more than a factor 2 larger as the one deduced from the OBE potential). This is in agreement with the observation that the modern OBE potentials are "softer" and contain a weaker tensor force as is also reflected in the D-state probability calculated for the deuteron [2].

Figure 2 also shows the prediction for the momentum distribution of nuclear matter obtained for the Reid soft-core potential using the much more sophisticated techniques of [18]. The good agreement of our approach, in which the self-energy is calculated in a perturbative scheme, including terms up to second order in G, with the one of [18], where the particle-particle hole-hole ladders are taken into account to all order using a self-consistent single-particle Greens function, gives us some confidence that the present approach provides reliable information for systematic studies in nuclear matter as well as finite nuclei.

The sensitivity of the calculated momentum distribution on the nuclear density is demonstrated in Fig. 3. In order to allow a direct comparison this figure does not show the momentum distribution but the occupation of the single-particle states as a function of the momentum k in units of the Fermi momentum (k/k_F). The results for the occupation of states below the Fermi momentum $(k/k_F \leq 1)$ are shown with respect to the linear scale on the left axis, while the occupation of states with momenta larger than k_F are shown with respect to the logarithmic scale on the axis at the right hand side. One observes that the calculated occupations are rather insensitive to density of the nuclear system. Only for very small densities $(k_F = 0.8$ fm^{-1}, which corresponds to roughly 20% of the empirical saturation density) does one find occupation probabilities which are considerably smaller. This might be an indication of the instability of homogeneous nuclear matter at such small densities [23,24].

In order to explore the density dependence a bit more in detail, we have separated the contributions to the single-particle density into a quasihole contribution and a continuum contribution. For momenta k below the Fermi momentum a large contribution to the momentum distribution of Eq. (15) originates from one eigenstate α with a maximal coefficient X_α and an eigenvalue ω_α which we identify as the quasihole energy $E_{qh}(k)$. In particular at small momenta $(k \approx 0.2 k_F)$ one also finds that a few states around the quasihole energy exhibit large coefficients X_α and therefore contribute significantly to the sum in Eq. (15). We define the quasihole strength to be the contribution of all terms in Eq. (15) which originate from an eigenstate of Eq. (14) with an eigenvalue within an interval of length 3 MeV around the quasihole energy E_{qh}:

$$N_{qh}(k) = \sum_\alpha \Theta(E_F - \omega_\alpha)\Theta(E_{qh}(k) + 1.5 - \omega_\alpha)$$

$$\times \Theta(\omega_\alpha - E_{qh}(k) + 1.5)X_\alpha^2. \qquad (40)$$

For momenta k larger than the Fermi momentum the eigenvalue of the state with maximal expansion coefficient X_α occurs at energies above the Fermi energy E_F and therefore we do not obtain any quasihole strength for those momenta. The quasihole strength N_{qh} is shown in Fig. 4 as a function

of the ratio k/k_F for two densities (lines labeled with triangles). The remaining contributions to the sum in Eq. (15) will be called the continuum contribution to the occupation probability or momentum distribution.

From the inspection of the results displayed in Fig. 4 one finds that the quasihole contribution to the occupation probability increases drastically with the momentum while the continuum contribution decreases in a corresponding way. A typical ratio of the quasihole versus continuum contribution is 0.6 for small momenta but as large as 10 for momenta close to the Fermi momentum. This means that the energy distribution of the single-particle strength is highly localized at the quasihole energy for states with momenta close to k_F whereas one observes a broad distribution and fragmentation of the strength for small momenta, i.e., deeply bound hole states.

The continuum contribution to the occupation probability decreases monotonically with increasing momentum and is a rather smooth function even at the Fermi momentum. This implies that the gap in the momentum distribution exhibited, e.g., in Fig. 2 at $k = k_F$ originates simply from the fact that the quasihole contribution vanishes since the energy of the corresponding state gets larger than the Fermi energy. It is worth noting that about 70% of the single-particle strength is located in the quasihole contribution. Two-thirds of the remaining continuum contribution occurs at momenta below the Fermi momentum and only one-third of the continuum contribution, which means slightly more than 10% of the total strength occurs at momenta above k_F.

From the single-particle Green's function we also determine the mean value of the energy for the spectral distribution at a given momentum,

$$\bar{\omega}(k) = \frac{\frac{1}{\pi}\int_{-\infty}^{\epsilon_F} d\omega\, \omega\, \mathrm{Im}g(k,\omega)}{n(k)}, \qquad (41)$$

or translated into the tools we are using in our numerical treatment,

$$\bar{\omega}(k) = \frac{1}{\tilde{n}(k)} \sum_\alpha \omega_\alpha \Theta(E_F - \omega_\alpha)X_\alpha^2, \qquad (42)$$

with the occupation number $\tilde{n}$ calculated following Eq. (15). The summation in this equation can be truncated as discussed above to determine the mean value for the energy resulting from the continuum part of the momentum distribution.

Such mean values are presented in the right part of Fig. 5. One finds that these mean values for the continuum are more negative than the corresponding HF single-particle energies or the energies of the quasihole states, which are shown in the left part of Fig. 5 (note the different scales on the axes). Particularly at large momenta, above k_F where the continuum part represents the total momentum distribution, these mean values $\bar{\omega}(k)$ are very attractive. This implies that these high-momentum components of the momentum distribution occur predominantly at large excitation energies of the residual nuclear system, which corresponds to large miss-
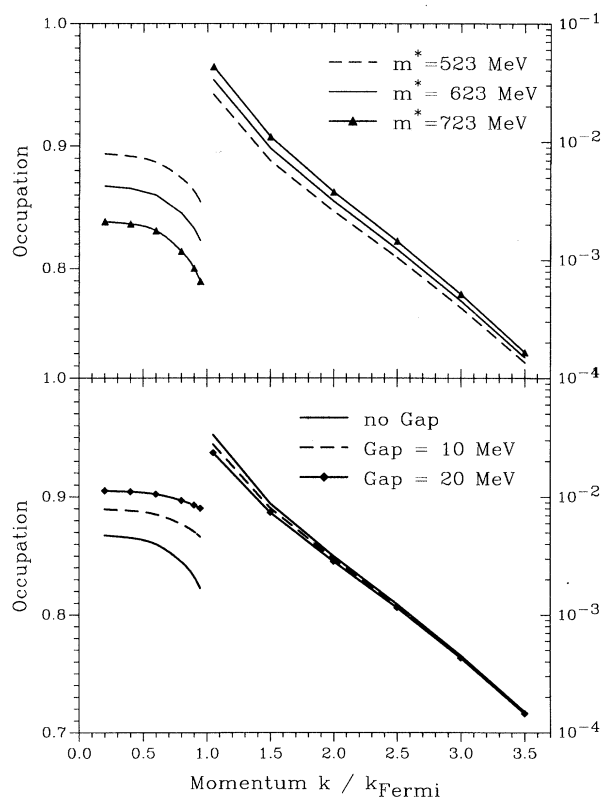
FIG. 6. Occupation probabilities in nuclear matter at $k_F = 1.35$ fm^{-1} using various modifications of the BHF single-particle spectrum.

FIG. 7. Occupation probabilities in nuclear matter at $k_F = 1.35$ fm^{-1} calculated in various BAGEL(n,m) approximations are compared to the result obtained with the complete Lehmann representation of the single-particle Green's function.

ing energies in knock out experiments. This result for nuclear matter confirms the observations made for finite systems in [26,27].

In the left part of Fig. 5 the BHF single-particle energies (lines labeled with triangles) are compared to the energies E_{qh} of the quasihole energies. One can see that the inclusion of the 2h1p terms of Fig. 1(c) yields a repulsive contribution to the quasihole energy. This is especially true for states with momenta well below the Fermi momentum. This means that the removal energy for nucleon knockout experiments exciting states with large spectroscopic factor should be much smaller for these deeply bound states than predicted in BHF calculations.

As a last point in this subsection we would like to explore the sensitivity of the calculated momentum distribution on the HF single-particle spectrum. For that purpose we have modified the effective mass parameter m^* in the parametrization of Eq. (39) from the BHF value of $m^* = 623$ MeV [39] at $k_F = 1.35$ fm^{-1} by $\pm$ 100 MeV. From the upper part of Fig. 6 one can see that a reduction of the effective mass— i.e., the single-particle energy shows a stronger momentum dependence—yields a reduction of the correlation effect. This reduction of the correlations is indicated by an enhancement of the occupation of states with $k \leq k_F$ and a reduction of the high-momentum components. Another modification of the HF single-particle spectrum can be obtained by introducing a gap between the energies of particle and hole states. As one can observe from the lower part of Fig. 6 such a gap
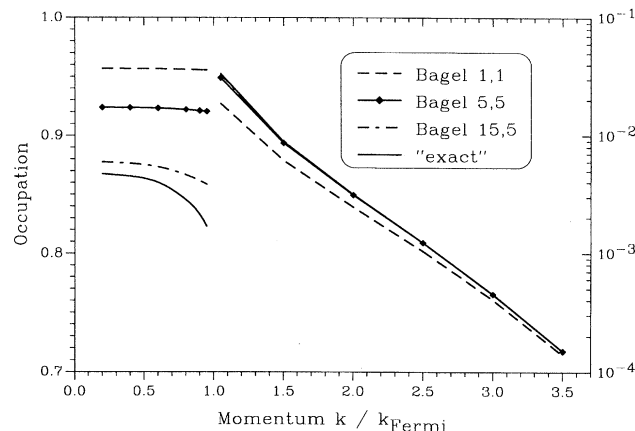
does not affect the high-momentum components very much but only the occupation probability around k_F.

B. BAGEL approximation

In order to investigate the efficiency of the BAGEL approximation introduced in the previous section for the representation of the single-particle Green's function in terms of a few poles we have evaluated the momentum distribution of nuclear matter considering various combinations BAGEL(n,m) for the number of basis states n in the 2p1h and m in the 2h1p part of the eigenvalue problem, Eq. (14). Results for a few examples are displayed in Fig. 7.

One finds that a very good approximation for the high-momentum components is obtained already with a very small number of basis states. The occupation probabilities for $k > k_F$ are reproduced in quite a satisfactory way in the simplest approximation BAGEL$(1,1)$ and the results become indistinguishable from the exact results if we use any approximation with n,m larger than 1. The convergence of the BAGEL approximation towards the exact result with increasing n,m is not as good for the occupation of states below k_F. A larger number of pole terms is required in particular to reproduce the decrease of the occupation number with k getting close to k_F.

Of course it is still a very efficient approximation to reduce the number of poles in the Lehmann representation of the single-particle Green's function of Eq. (13) from a few hundred obtained by an optimized discretization of the integrals in Eqs. (3) and (6) to $n + m + 1 = 21$ in the BAGEL$(15,5)$ approximation, but a closer inspection may help us to reduce the number of terms even more.

Analyzing the basis states which are generated by the BAGEL approach in the 2p1h part of the Hilbert space by applying $\hat{a}$ of Eq. (17) according to the Lanczos scheme, one observes that states are generated with very large eigenvalue ω_α but negligible amplitude X_α. It requires some iteration steps to generate a few states with lower energy and a non-negligible coefficient. This generation of basis states with extreme energies is of course a feature of the Lanczos ap-
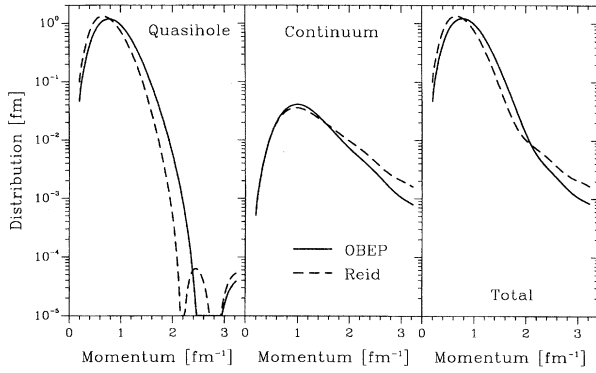
FIG. 8. Momentum distribution for ^{16}O in the $p_{1/2}$ partial wave [see Eq. (32)]. The distributions are normalized such that $\int dk\, n(k) = 1$ if one orbit would be occupied. The three parts of the figure display the quasihole contribution, the continuum contribution, and the sum of these two (total) as obtained for the OBE B (solid lines) and the Reid soft-core (dashed lines) potentials.

proach, which is not optimal for our present purpose. The situation is better for the generation of basis states in the 2h1p sector, as the eigenvalues of $\hat{A}$ [see Eq. (17)] are more limited.

From this discussion we see that the BAGEL approximation for the Green's function can be made more efficient by either ignoring the contributions of those poles in the Lehmann representation of Eq. (13), which show very small coefficients X_α, or replacing the Lanczos algorithm generating the basis states by one, which preferably generates eigenstates close to the Fermi energy.

C. Finite nuclei

As a first example for the momentum distribution calculated directly for the finite nucleus ^{16}O using the method described in [27] and briefly reviewed in Sec. III A, we present in Fig. 8 as a typical example the momentum distribution obtained for a $p_{1/2}$ partial wave. This refers to the corresponding contribution to the sum in Eq. (32) without the factor $2(2j+1)$ for degeneracy of these states. As in [27] we split the momentum distribution into a quasihole contribution, which should be observed if the $(A-1)$ nucleus remains in its ground state, and a continuum part reflecting the momentum distribution observed at larger missing energies.

The results obtained for the Reid soft-core potential [1] (dashed lines) are rather similar to those evaluated for the OBE potential B of [2] (solid lines). However, there are some characteristic differences which can also be observed in the other partial waves: The quasihole contribution evaluated for the Reid potential exhibits a maximum at smaller momenta and drops faster with increasing momentum. This reflects the fact that nuclear structure calculations like BHF yield less binding energy and a larger radius using the Reid soft-core potential as compared to the OBE model for the NN interaction. The continuum part, on the other side, exhibits larger contributions at high momenta using the Reid potential. Following the arguments present in the Introduction of this paper, this would be an indication that the Reid potential predicts "stronger" correlations.

TABLE I. Distribution of nucleons in ^{16}O. Listed are the occupation probabilities for various partial waves. These probabilities are obtained by integrating the partial wave contributions in Eq. (32) ignoring the degeneracy factors $2(2j+1)$. For states with $l \leq 1$ the contributions from the quasihole (n^{qh}) and the continuum part (n^c) of the spectral function are listed separately. Results have been obtained using the OBE potential B and the Reid soft-core potential.

	OBEP B		Reid	
lj	n^{qh}	n^c	n^{qh}	n^c
$s_{1/2}$	0.780	0.157	0.778	0.117
$p_{3/2}$	0.914	0.042	0.896	0.040
$p_{1/2}$	0.898	0.046	0.896	0.047
$d_{5/2}$		0.022		0.018
$d_{3/2}$		0.027		0.024
$f_{7/2}$		0.008		0.014
$f_{5/2}$		0.013		0.019
$g_{9/2}$		0.002		0.004
$g_{7/2}$		0.004		0.007

Another indicator for the importance of NN correlations are the occupation probabilities for the various partial waves as they are listed in Table I. These occupation probabilities are obtained by a momentum integration of the various partial wave contributions in Eq. (32). Again we distinguish between quasihole and continuum contribution for the partial waves with $l \leq 1$ and compare the results for the two models of the NN interaction. The results presented here for the OBE potential deviate slightly from those presented in [27] as we have increased the interval for the energy integration in Eq. (32) in our present study. It is interesting to note that the occupation probabilities are quite similar for both interactions for the orbits with angular momentum $l \leq 2$ with slightly larger values for the OBE potential. For the partial waves with larger l, however, the Reid potential predicts occupation probabilities which are significantly larger than those for the OBE potential. This difference seems to be due to the stronger tensor component contained in the Reid potential.

Multiplying the occupation probabilities of Table I with the degeneracy factors $2(2j+1)$ one finds that 2.05 (2.09, using Reid) "nucleons" out of the 16 for ^{16}O are represented by the continuum part of the momentum distribution. The total nucleon numbers, including the quasihole part, are 16.07 and 15.96 for the OBE and Reid potentials, respectively. This means that the particle-number-violating features of our present approach lacking a self-consistent treatment of the single-particle Green's function are not very strong [30].

The continuum part of the total momentum distribution including partial waves with $l \leq 4$ in the summation of Eq. (32) is displayed in the left part of Fig. 9. Again we can observe the characteristic differences obtained for the two interactions: While the OBE potential yields a momentum distribution which is slightly larger at small momenta, the Reid potential predicts contributions which are larger by almost a factor of 2 at large momenta. This is in complete
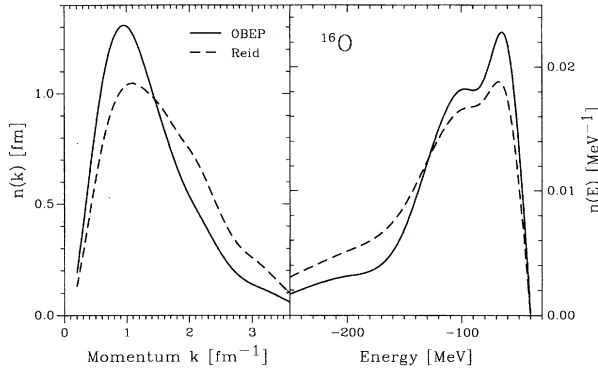
FIG. 9. Continuum part of the single-particle density for ^{16}O as a function of the momentum [left part; see Eq. (32)] and energy (right part). Results are presented as obtained for the OBE B (solid lines) and the Reid soft-core (dashed lines) potentials.

agreement with the observation made above for nuclear matter (see Fig. 2).

Figure 9 also exhibits the spectral distribution of the continuum part. This spectral distribution is obtained by replacing the energy integration in Eq. (32) by a momentum integration. One observes that the spectral distribution derived for the OBE potential is slightly larger at energies with small absolute value, which corresponds to small missing energies, while the Reid potential yields a larger result at large missing energies. Concluding we may characterize the differences between the two interactions by the following statement: The Reid potential predicts a larger component of the single-particle density at large momenta and large missing energies as compared to the OBEP potential B.

Finally, we would like to discuss the validity of the local-density approximation (LDA) introduced in Sec. III B. for the description of the momentum distribution at large momenta. Since this high-momentum part of the momentum distribution is dominated by the continuum contribution $\Delta n(k)$ in Eq. (36), we will restrict our discussion to this part and its comparison to the continuum part of the momentum distribution evaluated directly for finite nuclei.

The result for $\Delta n(k)$ calculated according to Eq. (35) using the OBE interaction is represented by the solid line in the left part of Fig. 10. In the discussion of the LDA above we already introduced a scheme to simulate the effects of a cutoff in the partial wave summation for the evaluation of the momentum distribution in finite nuclei. Comparing the prediction for the total $\Delta n(k)$ with those employing a restriction to a maximal orbital angular momentum, one observes that such a restriction leads to remarkable differences in particular at high momenta. Using $L_{max}=3$ in Eq. (38) one obtains a prediction for the momentum distribution, which is only one-half of the result including all partial waves at $k \approx 3.5$ fm^{-1}.

The right part of Fig. 10 shows the comparison of the continuum part of the momentum distribution evaluated directly for ^{16}O with the LDA prediction using $L_{max}=4$, the maximal orbital angular momentum, which we have taken into account in our direct evaluation for the finite system. The agreement of the LDA with the direct evaluation is very good in particular at high momenta. For small momenta the
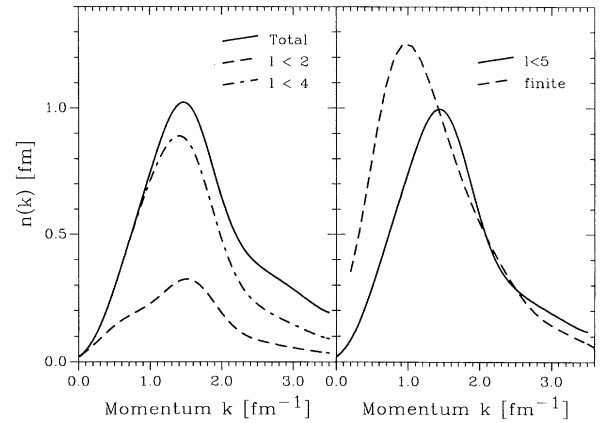

FIG. 10. Continuum part of momentum distribution for ^{16}O as obtained from the local-density approximation [see Eq. (35)] using the OBE potential B. In the left part of the figure the total contribution is compared to results obtained assuming various values L_{max} for the truncation of the partial wave expansion. The right part of the figure compares the local-density approximation with $L_{max}=4$ with the result obtained in a direct calculation of ^{16}O.

direct calculation for the finite system yields a larger value than the LDA. For these small momenta, however, one must keep in mind that the continuum part calculated directly for the finite system contains components which have a momentum distribution similar to the quasihole part [27], whereas the $\Delta n(k)$ evaluated in LDA only accounts for momenta above the local Fermi momenta $k_F(r)$.

Concluding we may say that the discrepancy observed in Ref. [27] between the predictions of high-momentum components in the single-particle density of nuclear matter and those for finite systems has been resolved. The LDA seems to produce very similar results if the same NN interaction is used, an appropriate average over nuclear matter with various densities is considered, and the effects of truncating the partial wave expansion in finite systems are taken into account.

V. CONCLUSIONS

The single-particle momentum distribution has been investigated for nuclear matter and the finite nucleus employing two different realistic models for the NN interaction. The investigations are based on the Green's function approach approximating the self-energy of the nucleon including all contributions up to second order in the G matrix. The main results can be summarized by the following conclusions.

(i) The present approach yields results for nuclear matter which are in very good agreement with the more elaborate calculations of [18]. This gives us some confidence that the same approximation should also produce reliable results if applied for finite systems.

(ii) The momentum distribution observed in knockout experiments with small missing energies should mainly observe the quasihole distribution with small components at high momenta. Larger contributions to the single-particle density at high momenta should be obtained at large excitation energies of the residual nucleus.

(iii) The prediction for the momentum distribution depend

weakly but in a rather characteristic way on the interaction used. The stronger tensor and short-range components of the Reid soft-core potential yield a larger single-particle strength at high momenta and large missing energies as compared to the OBE potential B of [2]. For momenta around 3.5 fm^{-1} the momentum distribution derived from the Reid interaction is larger by a factor 2 in nuclear matter as well as finite nuclei.

(iv) The momentum distribution calculated for finite nuclei is rather sensitive to a truncation in a partial wave expansion. Orbits with angular momenta l larger than 4 should be taken into account to obtain stable results at momenta $k \approx 4$ fm^{-1}.

(v) A local-density approximation, in which the high-momentum components in the single-particle density are derived from the study of correlations in nuclear matter, yields a very good agreement with corresponding studies for finite nuclei, if the effects due to truncations in the partial wave expansion are considered.

(vi) The numerical scheme developed for the solution of the Dyson equation in nuclear matter leads to a very efficient representation of the single-particle Green's function in terms of a few "characteristic" poles in the Lehmann representation. This BAGEL approximation could be very useful, e.g., in studies of nuclear response functions beyond the HF and random phase approximations.

ACKNOWLEDGMENTS

APPENDIX

This appendix lists the expressions [29] for the weighting function $W(q)$ and the average c.m. momentum $\tilde{K}_{av}$ which have been used in the calculation of the 2h1p contribution to the nucleon self-energy according to Eq. (6). For that purpose we distinguish four different cases of the momentum k for which the self-energy shall be evaluated:

$$\text{(a)} \quad 0 \leq k \leq \tfrac{1}{3} k_F,$$

$$\text{(b)} \quad \tfrac{1}{3} k_F < k < k_F,$$

$$\text{(c)} \quad k_F \leq k < 3k_F,$$

$$\text{(d)} \quad 3k_F \leq k < \infty. \tag{A1}$$

Case (a):

$$\tilde{K}_{av}(q,k) = \begin{cases} \dfrac{\tfrac{1}{3}\{(k+q)^3 + [\tfrac{1}{2}(k^2+k_F^2)-q^2]^{3/2}\}}{\tfrac{1}{4}(k^2-k_F^2)+q(q+k)} & \text{for } \tfrac{1}{2}(k_F-k) \leq q \leq \tfrac{1}{2}(k+k_F), \\[4mm] \dfrac{\tfrac{1}{3}[(q+k)^3-(q-k)^3]}{2kq} & \text{for } \tfrac{1}{2}(k+k_F) \leq q \leq (k_F-k), \\[4mm] \dfrac{\tfrac{1}{3}[(k_F)^3-(q-k)^3]}{\tfrac{1}{2}(k_F^2-k^2-q^2)+kq} & \text{for } (k_F-k) \leq q \leq (k+k_F), \end{cases} \tag{A2}$$

$$W(q) = \begin{cases} q\{\tfrac{1}{4}(k^2-k_F^2)+q(q+k)\} & \text{for } \tfrac{1}{2}(k_F-k) \leq q \leq \tfrac{1}{2}(k_F+k), \\[2mm] q\{2kq\} & \text{for } \tfrac{1}{2}(k_F+k) \leq q \leq (k_F-k), \\[2mm] q\{\tfrac{1}{2}(k_F^2-k^2-q^2)+kq\} & \text{for } (k_F-k) \leq q \leq (k_F+k). \end{cases} \tag{A3}$$

Case (b):

$$\tilde{K}_{av}(k,q) = \begin{array}{ll} \dfrac{\tfrac{1}{3}\{(k+q)^3 + [\tfrac{1}{2}(k^2+k_F^2)-q^2]^{3/2}\}}{\tfrac{1}{4}(k^2-k_F^2)+q(q+k)} & \text{for } \tfrac{1}{2}(k_F-k) \leq q \leq (k_F-k), \\[4mm] \dfrac{\tfrac{1}{3}\{k_F^3 - [\tfrac{1}{2}(k^2+k_F^2)-q^2]^{3/2}\}}{\tfrac{1}{4}(k_F^2-k^2)+1/2\,q^2} & \text{for } (k_F-k) \leq q \leq \tfrac{1}{2}(k+k_F), \\[4mm] \dfrac{\tfrac{1}{3}[(k_F)^3-(q-k)^3]}{\tfrac{1}{2}(k_F^2-k^2-q^2)+kq} & \text{for } \tfrac{1}{2}(k+k_F) \leq q \leq (k+k_F), \end{array} \tag{A4}$$

$$W(q) = \begin{cases} q\{\frac{1}{4}(k^2 - k_F^2) + q(q+k)\} & \text{for} \quad \frac{1}{2}(k_F - k) \leq q \leq (k_F - k), \\[2mm] k\left\{\frac{1}{4}(k_F^2 - k^2) + \frac{1}{2}q^2\right\} & \text{for} \quad (k_F - k) \leq q \leq \frac{1}{2}(k_F + k), \\[2mm] k\{\frac{1}{2}(k_F^2 - k^2 - q^2) + kq\} & \text{for} \quad \frac{1}{2}(k_F + k) \leq q \leq (k_F + k). \end{cases} \tag{A5}$$

Case (c):

$$\tilde{K}_{\mathrm{av}}(k,q) = \begin{cases} \dfrac{\frac{1}{3}\{k_F^3 - [\frac{1}{2}(k^2 + k_F^2) - q^2]^{3/2}\}}{\frac{1}{4}(k_F^2 - k^2) + 1/2\, q^2} & \text{for} \quad \sqrt{\frac{1}{2}(k - k_F)(k + k_F)} \leq q \leq \frac{1}{2}(k + k_F), \\[4mm] \dfrac{\frac{1}{3}[(k_F)^3 - |q - k|^3]}{\frac{1}{2}(k_F^2 - k^2 - q^2) + kq} & \text{for} \quad \frac{1}{2}(k + k_F) \leq q \leq (k + k_F), \end{cases} \tag{A6}$$

$$W(q) = \begin{cases} q\{\frac{1}{4}(k_F^2 - k^2) + \frac{1}{2}q^2\} & \text{for} \quad \sqrt{\frac{1}{2}(k - k_F)(k + k_F)} \leq q \leq \frac{1}{2}(k_F + k), \\[2mm] q\{\frac{1}{2}(k_F^2 - k^2 - q^2) + kq\} & \text{for} \quad \frac{1}{2}(k_F + k) \leq q \leq (k_F + k). \end{cases} \tag{A7}$$

Case (d):

$$\tilde{K}_{\mathrm{av}}(k,q) = \begin{cases} \dfrac{\frac{1}{3}[(k_F)^3 - |q - k|^3]}{\frac{1}{2}(k_F^2 - k^2 - q^2) + kq} & \text{for} \quad (k - k_F) \leq q \leq (k + k_F), \end{cases} \tag{A8}$$

$$W(q) = \{q\{\frac{1}{2}(k_F^2 - k^2 - q^2) + kq\} \quad \text{for} \quad (k - k_F) \leq q \leq (k_F + k). \tag{A9}$$

[1] R.V. Reid, Ann. Phys. (N.Y.) **50**, 411 (1968).

[2] R. Machleidt, Adv. Nucl. Phys. **19**, 189 (1989).

[3] H. Müther, Prog. Part. Nucl. Phys. **17**, 97 (1986).

[4] P. Ring and P. Schuck, *The Nuclear Many-Body Problem* (Springer, New York, 1980), Appendix D.

[5] B. Dreher, J. Friedrich, K. Merle, H. Rothhaas, and G. Lührs, Nucl. Phys. **A235**, 219 (1974).

[6] C.J. Batty, E. Friedman, H.J. Gils, and H. Rebel, Prog. Part. Nucl. Phys. **17**, 1 (1986).

[7] L. Lapikas, Nucl. Phys. **A553**, 297c (1993).

[8] I. Bobeldijk *et al.*, Phys. Rev. Lett. **73**, 2684 (1994).

[9] K.I. Blomqvist *et al.*, Phys. Lett. B **344**, 85 (1995).

[10] H. Morita and T. Suzuki, Prog. Theor. Phys. **86**, 671 (1991).

[11] S. Tadokoro, T. Katyama, Y. Akaishi, and H. Tanaka, Prog. Theor. Phys. **78**, 732 (1987).

[12] C. Ciofi degli Atti, E. Pace, and G. Salmè, Phys. Lett. **141B**, 14 (1984).

[13] O. Benhar and V.R. Pandharipande, Phys. Rev. C **47**, 2218 (1993).

[14] C. Mahaux and R. Sartor, Adv. Nucl. Phys. **20**, 1 (1991).

[15] A. Ramos, A. Polls, and W.H. Dickhoff, Nucl. Phys. **A503**, 1 (1989).

[16] O. Benhar, A. Fabrocini, and S. Fantoni, Nucl. Phys. **A505**, 267 (1989).

[17] C. Ciofi degli Atti, S. Simula, L.L. Frankfurt, and M.I. Strikman, Phys. Rev. C **44**, R7 (1991).

[18] B.E. Vonderfecht, W.H. Dickhoff, A. Polls, and A. Ramos, Nucl. Phys. A **555**, 1 (1993).

[19] C.C. Gearhart, W.H. Dickhoff, A. Polls, and A. Ramos (unpublished).

[20] M. Baldo, I. Bombaci, G. Giansiracusa, U. Lombardo, C. Ma-
haux, and R. Sartor, Phys. Rev. C **41**, 1748 (1990).

[21] H.S. Köhler, Nucl. Phys. **A537**, 64 (1992).

[22] S. Stringari, M. Traini, and O. Bohigas, Nucl. Phys. **A516**, 33 (1990).

[23] D. van Neck, L. Dieperink, and E. Moya de Guerra, Phys. Rev. C **51**, 1800 (1995).

[24] O. Benhar, A. Fabrocini, S. Fantoni, and I. Sick, Nucl. Phys. **A579**, 493 (1994).

[25] S.C. Pieper, R.B. Wiringa, and V.R. Pandharipande, Phys. Rev. C **46**, 1741 (1992).

[26] H. Müther and W.H. Dickhoff, Phys. Rev. C **49**, R17 (1994).

[27] H. Müther, A. Polls, and W.H. Dickhoff, Phys. Rev. C **51**, 3040 (1995).

[28] M.I. Haftel and F. Tabakin, Nucl. Phys. **A158**, 1 (1970).

[29] G. Knehr, diplom thesis, Universität Tübingen, 1994.

[30] W.H. Dickhoff and H. Müther, Rep. Prog. Phys. **55**, 1947 (1992).

[31] H. Müther and L.D. Skouras, Nucl. Phys. **A555**, 541 (1993).

[32] H. Müther and L.D. Skouras, Nucl. Phys. **A581**, 247 (1995).

[33] H. Müther, T. Taigel, and T.T.S. Kuo, Nucl. Phys. **A482**, 601 (1988).

[34] J.H. Wilkinson, *The Algebraic Eigenvalue Problem* (Oxford University Press, New York, 1965).

[35] M. Borromeo, D. Bonatsos, H. Müther, and A. Polls, Nucl. Phys. **A539**, 189 (1992).

[36] M.G.E. Brand, G.A. Rijsdijk, F.A. Muller, K. Allaart, and W.H. Dickhoff, Nucl. Phys. **A531**, 253 (1991).

[37] G.A. Rijsdijk, K. Allaart, and W.H. Dickhoff, Nucl. Phys. **A550**, 159 (1992).

[38] H. Müther and L.D. Skouras, Phys. Lett. B **306**, 306 (1993).

[39] R. Brockmann and R. Machleidt, Phys. Rev. **C42**, 1965 (1990).